Soft Matter

Accepted Manuscript

ROYAL SOCIETY OF CHEMISTRY

www.rsc.org/softmatter

Yielding and Flow of Cellulose Microfibril Dispersions in the Presence of Charged Polymer

Daan W. de Kort[a,b], Sandra J. Veen[c], Henk Van As[a,b], Daniel Bonn[d], Krassimir P. Velikov[c,e], John P.M. van Duynhoven[a,b,c,*]

[a]Laboratory of Biophysics, Wageningen University, Dreijenlaan 3, 6703 HA Wageningen, The Netherlands

[b]TI-COAST, Science Park 904, 1098 XH Amsterdam, The Netherlands

[c]Unilever R&D, Olivier van Noortlaan 120, 3133 AT Vlaardingen, The Netherlands

[d]Van der Waals-Zeeman Institute, IoP, University of Amsterdam, Science Park 904, 1098 XH Amsterdam, The Netherlands

[e]Soft Condensed Matter, Debye Institute for Nanomaterials Science, Utrecht University, Princetonplein 5, 3584 CC Utrecht, The Netherlands

*Corresponding Author

Graphical Abstract

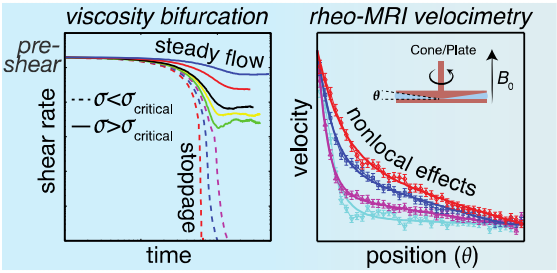

Abstract

Shear flow of microfibrillated cellulose dispersions is still not wholly understood as a consequence of their multi-length-scale heterogeneity. We added carboxymethyl cellulose, a charged polymer, to make cellulose microfibril dispersions more homogeneous at the sub-micron and macro scales. We then compared the yielding and flow behavior of these dispersions to that of typical thixotropic yield-stress fluids. Despite of their apparent homogeneity, the velocity profiles of the dispersions in cone-plate geometry, as measured by rheo-MRI velocimetry, differ strongly from those observed for typical thixotropic model systems: the viscosity across the gap is not uniform, despite a flat stress field across the gap. We describe these velocity profiles with a nonlocal model, and attribute the non-locality to persistent micron-scale structural heterogeneity.

1. Introduction

Dispersions of cellulose microfibrils (MFs) have received considerable attention as sustainable and natural materials with applications ranging from coatings and packaging materials to foods and cosmetics.[1] Their long, anisotropic shape allows the MFs to be used as scaffolding in polymer nanocomposites.[2] For such composite gels, emphasis lies on their elastic properties, although their flow properties are also relevant, for instance for industrial processing and behavior during consumer use. A major obstacle in understanding flow is the compositional and structural heterogeneous nature of these dispersions.

Cellulose MF dispersions are commonly prepared from native plant cellulose fibers by homogenization under very high pressures (~MPa), separating the fibers into their constituent MFs.[3] Plant cellulose MFs have a high aspect ratio, leading to a low percolation threshold and gelation already at low concentrations.[4] Various strains of bacteria exist that excrete a chemically well-defined form of cellulose MFs. This bacterial cellulose (BC) is excreted as twisting ribbons, with diameters in the nanometers range and lengths of several micrometers. Bacterial cellulose has no functional groups other than hydroxyl groups.[1,5] Although bacterial cellulose microfibrils (BCMF) are still polydisperse in size and width, we use them as model systems for microfibrillated plant cellulose because of their well-defined chemical properties.

Cellulose MFs have a strong tendency to aggregate due to Van der Waals and hydrogen bond driven interactions.[6] BCMFs have only a low ζ-potential (–7.5 mV), which is too low to stabilize them in aqueous suspensions, leading to their flocculation and sedimentation.[7,8] Optical setups were used to measure floc sizes in MFPC dispersions under shear.[9-11] It was shown that, in a Taylor-Couette or concentric cylinders (CC) geometry at low MF concentrations (0.1-0.25 wt%) and low shear rates (0.5 s^{-1}), the fibers accumulated into log-rolling cylinders aligned in the vorticity direction. This effect was not observed in more concentrated dispersions (>1 wt%), where the MFs remained more homogeneously distributed as flocs. The size of the flocs has been measured as a function of shear rate and was on the order of 0.1-1 mm, and typically decreased with shear rate. The presence of flocs

lead to a depleted layer at the wall, because the centers of particles (flocs) can only approach the walls to within a distance equal to their radius.[12] This was visualized directly by Nechyporchuk et al., who used an optical setup to study flow of MF dispersions in cone-and-plate (CP) geometry.[13] Under shear, a fast-moving water layer formed close to the cone due to the release of water from the bulk of the dispersion. Martoïa et al. used ultrasonic velocimetry to measure flow profiles within a CC geometry.[14] They observed that the flow profile was banded and additionally that the flow profile was not uniform in the vorticity direction and strongly time dependent. Similar turbulent flow was observed in early MRI velocimetry studies, which was attributed to the strongly heterogeneous floc distribution.[15,16]

Addition of carboxymethyl cellulose (CMC), a negatively charged cellulose derivative, to BCMF dispersions and subsequent homogenization partly reversed flocculation. CMC is thought to interact with cellulose mainly through hydroxyl-mediated hydrogen bonding.[17-19] This results in stable gels with partly aligned MFs, depending on their concentration and the BCMF/CMC ratio.[8] In these gels, the distribution of MFs over the available volume is homogeneous at the sub-micron length scale as observed by electron microscopy.[20] These microstructural effects are accompanied by an increase in the magnitude of the elastic modulus. After loading the sample onto the rheometer, the elastic modulus gradually increased with time, suggesting that an MF network that has been broken down by shear can spontaneously recover in time.[20] Although thixotropic behavior has been demonstrated for pristine BCMF dispersions[21,22] it has not been clearly established for BCMF/CMC systems. The observations of the increase of the elastic modulus in time indicate that the rheology of BCMF/CMC is similar to that of pristine BCMF dispersions, the difference being that the latter is much more heterogeneous than the former. In order to address the hypothesis that BCMF/CMC dispersions are homogeneous thixotropic fluids, we will carry out a detailed investigation of their flow behavior. We will work in the regime where the concentration of MFs is high enough to form a percolating, arrested network, and high enough levels of CMC to prevent significant aggregation and sedimentation. Such conditions can be found at BCMF/CMC weight ratios lower than ~5 at MF weight fractions higher than

0.1 wt%.[8] Viscosity bifurcation measurements will be used to establish the critical stress where MF network breakage (shear rejuvenation) is balanced by reformation. Next we will use rheo-MRI velocimetry to study flow of BCMF/CMC dispersions close to the critical stress[23,24] and compare with the behavior of typical thixotropic yield stress fluids[25].

2. Experimental procedures

Sample preparation

Cubes of BC in syrup from eight cups with 220 mL of lychee/vanilla flavored nata de coco (Kara Santan Pertama, Bogor 16964, Indonesia) were filtered and washed under a demi-water tap. After immersion in 1.5 L of nanopure water (Barnstead Nanopure Diamond, conductivity 18 µS/cm) the cubes were cut by a hand blender (Braun 4185545) and washed. Each washing step consisted of rinsing the cellulose by filtration over a vacuum filter (Whatman Schleicher and Schuell 113, wet strengthened circles, 185 mm diameter) and redispersing the residue in 1.5 L of nanopure water with the hand blender. After eight washing steps the cellulose residue was redispersed in 400 mL of nanopure water. Several samples containing 0.8 wt% BCMF were prepared by dilution with nanopure water and adding different amounts of a concentrated CMC solution (Ashland Blanose Aqualon 99.5% pure, 9M31XF, $M_w \approx 250$ kg/mol, degree of polymerization 1100, degree of substitution 0.80-0.95, density 0.75 kg/L). These samples were passed through a Microfluidizer once (M110S, Microfluidics) with a *z*-chamber of 87 µm at a pressure of 120 MPa. The weight fraction of BCMF in the resulting mixtures was determined gravimetrically by drying of the dispersions under reduced pressure and elevated temperatures. The average over three samples per CMC/BCMF ratio was taken. Dilutions were made by addition of nanopure water and redispersion by gentle shaking.

Rheology

Apparatus. Experiments were performed on an Anton Paar Physica MCR301 rheometer equipped with (1) a CP geometry, cone angle 2.0°, cone diameter 4 cm, truncation gap 60 μm and (2) a serrated CC (PEEK) geometry, r_i/r_o 8.5/9.5 mm (gap width 1.0 mm).

Flow curves (strain controlled). Flow curves of BCMF/CMC 0.80/0.15, 0.80/0.20 and 0.20/0.05 wt% were measured under strain controlled conditions. In CP geometry, we performed a test with an up- and down sweep in shear rate. The shear rate was first increased from 0.1 to 500 s^{-1} in 2 min and then decreased from 500 to 0.1 s^{-1} in 2 min. In CC geometry, a flow curve of BCMF/CMC 0.20/0.05 wt% was measured. The shear rate was decreased from 2×10^{2} to 2×10^{-3} s^{-1} over the course of 1h, after pre-shearing the sample at 200 s^{-1} for 3 minutes.

Viscosity bifurcation (stress controlled) measurements. For these experiments we used CC geometry and BCMF/CMC 0.20/0.05 wt% dispersions. In each experiment a fresh sample was used that was pre-sheared at 200 s^{-1} for 3 minutes after which a fixed stress was applied. The rate of strain was then measured as a function of time.

Rheo-MRI velocimetry

Time-averaged velocity profiles were measured according to procedures by Callaghan et al.[26,27] on a Bruker Avance II spectrometer at 7.0 T magnetic field strength (resonance frequency 300 MHz for ^{1}H). The magnet was equipped with a Bruker rheo-MRI accessory in combination with two measurement geometries: (1) a CP, cone angle 7.0°, cone diameter 1 cm (PEEK) and (2) a serrated CC, r_i/r_o 8.5/9.5 mm (PEEK).

3. Results and discussion

Addition of small amounts of CMC to a BCMF dispersions not only leads to a more homogeneous distribution of MFs at the sub-micron scale (SI, section 1a), but also to significant improved stability against aggregation. For plain dispersions of BCMF, mild shear induces a log-rolling effect, which is absent when CMC is added. This can be visualized by imaging the local density of BCMC using MRI

R_2 contrast when dispersions with and without CMC are sheared in a CC geometry, as is shown in Figure 1. The BCMF/CMC dispersion shows no sign of such shear-induced heterogeneities and appears homogeneous at the rheometer (macro)scale.

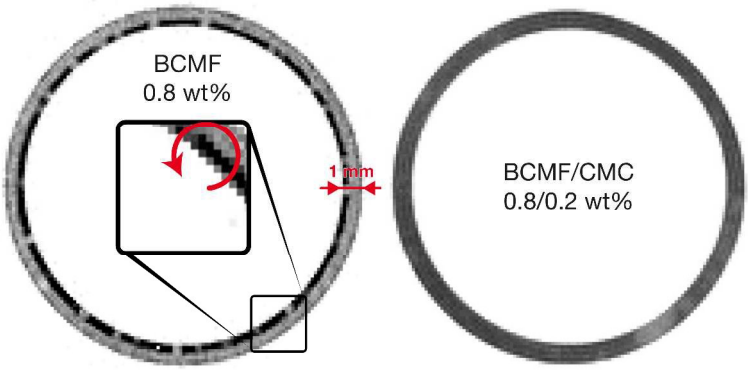

Figure 1. R_2-contrast MRI images of the annulus of a r_i/r_o 8.5/9.5 mm CC geometry after mild pre-shear of 5/s during 3 minutes (slice thickness 1.0 cm). The presence of cellulose MFs leads to faster relaxation of the NMR signal and hence to a larger R_2-value (i.e., brighter areas contain more MFs). Under these circumstances, no strong contrast can be observed in the BCMF/CMC dispersion, while in the BCMF dispersion large flocs (logs) have formed that span part of the gap.

In strain-controlled flow curves of BCMF/CMC dispersions (Figure 2), we can see that the dispersions are strongly shear thinning, and that the concentrations of MFs and CMC are (unsurprisingly) reflected in the bulk viscosity.

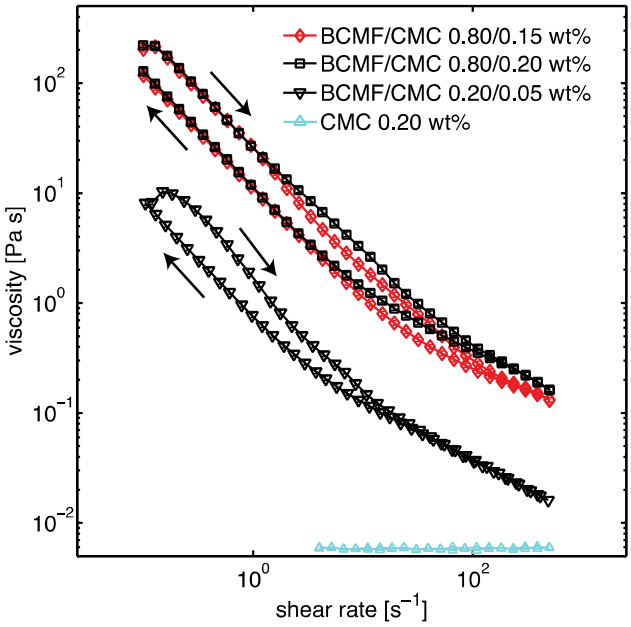

Figure 2. Strain-controlled macroscopic flow curves of dispersions of different BCMF concentrations and BCMF/CMC ratios. The shear rate was first increased from 0.1 to 500 s^{-1} in 2 min and then decreased from 500 to 0.1 s^{-1} in 2 min (see arrows). The viscosity of CMC 0.2 wt% could only be determined in part of this domain due to limited sensitivity of the rheometer.

Higher MF concentrations lead to an upward shift in viscosity of the whole flow curve, whereas the viscosity effect of CMC can only be seen at higher shear rates. Local measurements of the apparent viscosity of the continuous phase from the mobility of nanoparticles by diffusion NMR[28-31], and an assessment of the molecular mobility of CMC by ^{1}H NMR spectroscopy show that at most 5% of CMC closely associates with the MFs, while the rest remains dissolved in solution (SI, section 1b). In the high shear rate regime, the dispersive effect of the addition of CMC leads to an increase of bulk viscosity significantly larger than only the contribution of the viscosity of the continuous phase (which is < 6 mPa).

The down-sweep flow curve shows lower viscosities than the up-sweep, and this behavior repeats for every successive sweep. In other work, the time-dependent rheology and thixotropy of cellulose MF dispersions has been demonstrated.[22,32] The viscosity decrease seen in Figure 2 is therefore likely caused by the thixotropy of the dispersions, implying that flow curves measured by a shear rate

sweep (such as in Figure 2) do not necessarily reflect steady-state properties. Assuming the MF dispersions are indeed thixotropic, we need to monitor the development of the viscosity under a single imposed stress as a function of time in order to measure the steady-state flow properties of the dispersions.

Viscosity bifurcation behavior. Thixotropy and yield-stress are both associated with the continuous breakage and reformation of the particle (fiber) network and are therefore thought to be intrinsically linked.[23,24] In steady state, under a constant stress, a kinetic balance between network breakage (shear rejuvenation) and reformation (aging) determines whether or not a thixotropic yield stress fluid can flow. There exists a critical stress σ_c, above which shear rejuvenation outcompetes aging so that the fluid can flow homogeneously, and below which aging outcompetes shear rejuvenation, eventually resulting in an infinite viscosity (i.e., in a solid) and no flow, even if the material was flowing initially. This phenomenon is known as the viscosity bifurcation[23], and implies that in steady state, under controlled stress, a wide range of shear rates is inaccessible, namely those shear rates below the critical shear rate $\dot{\gamma}_c$, which is the shear rate at the critical stress $\dot{\gamma}(\sigma_c)$.

To demonstrate this behavior for cellulose microfibril dispersions, we performed viscosity bifurcation experiments for a selected BCMF/CMC dispersion (0.20/0.05 wt%) in CC geometry. In these experiments, we monitored the shear rate as a function of time under a fixed stress. Immediately prior to each experiment, we erase the shear history of the sample by a shearing at 200 s^{-1} for three minutes. We compare the resulting steady-state shear rates with flow curves acquired through a slow strain sweep. The results are presented in Figure 3.

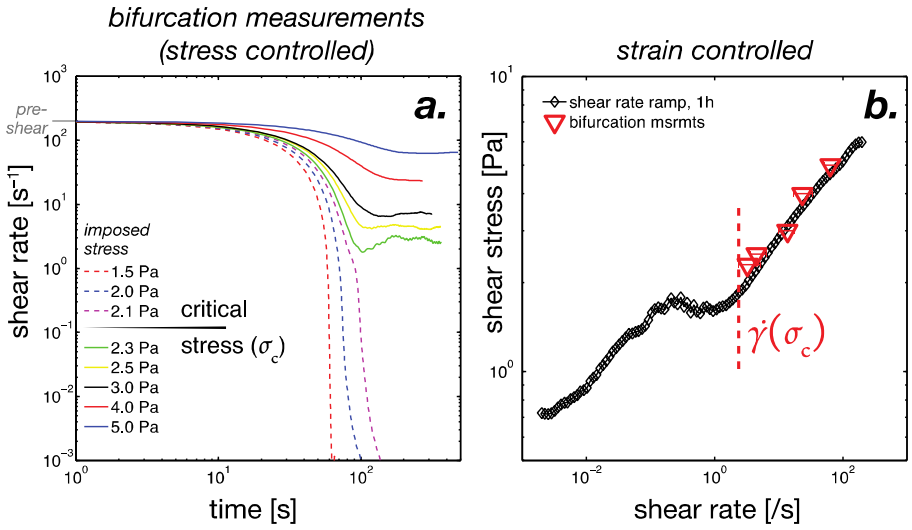

Figure 3. (*a*) Viscosity bifurcation measurements on BCMF/CMC 0.20/0.05 wt% in CC geometry. Before imposing constant stress, the dispersions were pre-sheared at 200 s^{-1} for three minutes. **(*b*)** Results of the viscosity bifurcation experiments superimposed onto a slowly acquired (1 h) strain-sweep flow curve. The apparent critical shear rate $\dot{\gamma}_c$ is indicated with a dotted line.

The existence of a critical stress is evident from the viscosity bifurcation experiments (Figure 3a), which show that below a critical stress the initial flow of the fluid comes to a halt (dotted lines). For stresses higher than the critical stress, the shear rate develops towards a steady state value (solid lines). We can overlay these steady-state shear rates onto a flow curve that was obtained by slow a strain sweep, so that it should be close to steady state behavior. The slowly acquired strain-sweep flow curve of Figure 3b is very similar to flow curves of cellulose MF dispersions previously presented in the literature (e.g., ref [14]). We find that the steady-state shear rates from the stress-controlled experiments overlap with this strain-controlled flow curve. However, a wide range of shear rates below the apparent critical shear rate $\dot{\gamma}(\sigma_c)$ is inaccessible under stress-controlled conditions. Moreover, one would expect strain-controlled flow curves to be flat below the critical shear rate, as demonstrated for instance for dispersions of mildly attractive silica particles by Møller et al.[25] The unusual features that can be seen in the flow curves (such as the negative slope at shear rates around 10 s^{-1}) cannot be accounted for by the viscosity bifurcation model or the more conventional

Herschel-Bulkley model, which describe typical flow curves of yield-stress fluids. Effects similar to those seen in Figure 3b have been described by Ovarlez et al. as typically occurring below the critical stress in some soft-jammed materials.[33] In such cases, the observation of a stress plateau within limited range of shear rates is typically caused by shear localization within a thin layer in the material. Because our cellulosic material might not be a jammed system for which reason we should be careful to apply such conclusions directly to this material, we measured flow profiles (velocity as a function of position in the gap) in order to check whether the flow is indeed localized in only a narrow part of the sample.

*Nonlocal effects***.** Thixotropic yield stress fluids flowing profiles in homogeneous stress fields typically have a perfectly linear flow profile at imposed shear rates $>\dot{\gamma}_c$, i.e., there is a single shear rate across the gap. In case a shear rate $<\dot{\gamma}_c$ is imposed upon the material, it accommodates this deformation through shear banding: One shear band flows with shear rate $\dot{\gamma}_c$; This band can not span the whole gap, so that part of the material does not move ($v = 0$).[25]

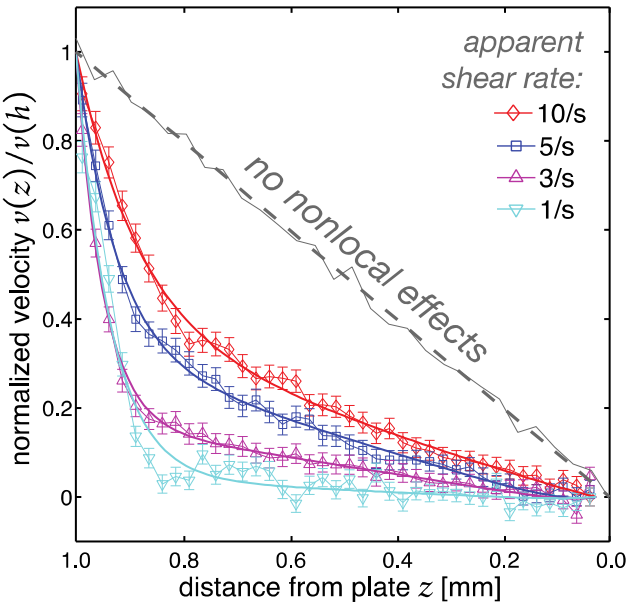

Figure 4. Flow profiles (velocity normalized to the cone velocity) of BCMF/CMC 0.20/0.05 wt% in CP geometry. Solid lines are fits to the nonlocal model.[34] The gap is 1.0 mm wide at the position where the profile is measured. The CP geometry is not sandblasted, which leads to slippage at the plate (i.e., the velocity drops

to zero over a very small distance, cf. SI, section 2). By extrapolation of the last five pixels at the plate (as in ref [34]), we could correct the flow profile for the slippage. The dashed line represents the flow profile of non-thixotropic yield stress fluids such as dense suspensions of soft particles in a homogeneous stress field with a gap much larger than the particle size.[35] Indeed, the flow profile of a hair gel containing carbopol (in gray) is linear, implying the absence of non-locality.

We measured such (time-averaged) flow profiles by rheo-MRI velocimetry (Figure 4). A 7° CP geometry was used, because here the spatial variation of the stress across the gap $\sigma(z)$ is only 1.5%[36] and can be safely ignored[25], unlike for flow in CC geometry or in pipes[16]. The flow profiles were measured in the shear rate regime close to the critical shear rate (~1–10 s^{-1}). Since the local viscosity $\eta(z)=\frac{\sigma_0}{\dot{\gamma}(z)}$, where σ_0 is the (nearly) z-independent stress, and the local shear rate in CP geometry $\dot{\gamma}(z)=\frac{\partial v(z)}{\partial z}$, the strong non-linearity of the flow profiles in Figure 4 directly reflects local viscosity differences across the gap. The flow profiles thus differ strongly from the typical picture, where for shear rates (a) higher than $\dot{\gamma}_c$ the flow profile is linear or (b) lower than $\dot{\gamma}_c$ the flow profile is banded into a region without flow and a region with shear rate $\dot{\gamma}_c$.[25] In our case, there is flow throughout the gap, while the local shear rate is not constant. This implies that the viscosity varies spatially across the gap.

A recent model by Goyon et al.[34] can account for such spatial variation of the viscosity. The model introduces a length scale ξ at which nonlocal effects can lead to spatial variations in the viscosity even if the stress is homogeneous.[37] Fluidity is the reciprocal of viscosity, and its spatial variation can be described as $f(z)=f_{bulk}+\xi^2\frac{\partial^2 f(z)}{\partial z^2}$, where f_{bulk} is the fluidity of the bulk and ξ a flow cooperativity length. Different explanations have been given as to the physical meaning of the cooperativity length, depending on the type of material studied, suggesting that it is the distance over which plastic events influence each other[38], but that it is not necessarily a material property[39]. Ignoring the minor spatial

variation of the stress in our CP geometry, we can integrate over z to obtain an expression for the velocity across the gap (no-slip boundary conditions, cf. SI, section 3):

$$v(z)= \sigma_0 f_{\text{bulk}} z+\sigma_0\left(f_{z=0}-f_{\text{bulk}}\right)\xi \sinh\left(\frac{z}{\xi}\right)+\frac{v(h)-\sigma_0 f_{\text{bulk}} h-\sigma_0\left(f_{z=0}-f_{\text{bulk}}\right)\xi \sinh\left(\frac{h}{\xi}\right)}{\cosh\left(\frac{h}{\xi}\right)-1}\left[\cosh\left(\frac{z}{\xi}\right)-1\right],$$

where h is the local height of the gap, $v(h)$ the velocity of the cone, $f_{z=0}$ the fluidity at the plate, and σ_0 the homogeneous stress. The model accounts for the observed spatial variation of the viscosity with a flow cooperativity length ξ of 0.08 ± 0.03 mm. Nonlocal effects have been observed in cases where the flow of a fluid is strongly confined, i.e., the width of the channel or gap in which the fluid flows is only one or two decades larger than the size of the dispersed particles. In BCMF gels in absence of CMC, at 0.20 wt% MF concentration, there is a broad, lognormal floc size distribution in the 1-100 µm range with a medium floc size of 15 µm.[7] The length scale of these heterogeneities is comparable to ξ, implying that these heterogeneities might persist in BCMF dispersions even after addition of CMC. This could effectively render the dispersions confined within the CP geometry, as the gap at the measurement position is 1.0 mm wide. Although the presence of CMC makes the dispersions clearly more homogeneous the submicron scale and mitigates progressive macroscale aggregation of the microfibrils (Figure 1), it apparently does not lead to completely homogeneous dispersions at the micron scale. Another explanation for the observed non-locality could be migration or dilatation of such micron-size particles under shear, leading to density differences and consequently viscosity differences across the gap. Such effects have been observed for granular materials and suspensions with element sizes on the order of the gap width.[39,40] This explanation might still be consistent with the homogeneous density of the BCMF/CMC dispersion as shown in Figure 1 (measured in the absence of shear), if the density differences that arise under shear quickly disappear after flow has stopped.

The shear rates imposed when measuring the flow profiles presented in Figure 4 were similar to the critical shear rate $\dot{\gamma}_c$ found by the viscosity bifurcation experiments. This means that, due to the strong

curvature of the flow profiles, the local shear rate, which is given by the slope of the flow velocity profiles particularly at the lower imposed shear rates, drops significantly below $\dot{\gamma}_c$. This is not consistent with the picture that the local shear rate cannot be lower than $\dot{\gamma}_c$. Apparently, the sharp transitions between sheared and stationary regions as observed for typical thixotropic yield-stress fluids in CP geometry do not occur for cellulose, and are apparently broadened, as observed for granular media.[40,41] This might also underlie the continuation of the strain-controlled flow curve of Figure 3b below the apparent critical shear rate. To distinguish between those cases would require a study of a granular material with a well-defined particle size on the order of the gap width in a homogeneous stress field at shear rates close to the critical shear rate.

As recently demonstrated by Paredes et al.[42], nonlocal effects due to the presence of large particles should be distinguished from wall slip due to the non-affinity of particles with the wall, for which can be corrected before the nonlocal model is applied[34]. True wall slip of cellulose MF dispersions is notoriously difficult to be prevented in typical rheometer setups, because of the weak affinity of the cellulose fibers with most surfaces, and possibly depletion effects. Both wall slip and nonlocal effects, however, contribute to the macroscopic observation of wall slip. Such apparent wall slip can be observed by varying the gap width in PP geometry, and is indeed significant in the case of BCMF dispersions (cf. SI, section 4). The relative contributions of true wall slip and nonlocal effects to the apparent macroscopic wall slip will vary as a function of applied stress and cannot be predicted.

Conclusions

Although CMC adsorbs only partly to cellulose MFs, addition of CMC leads to a significantly more homogeneous colloid at the sub-micron and macroscopic scales. For this reason we expected the flow behavior of BCMF/CMC dispersions to resemble that of microscopically homogeneous thixotropic fluids. We first showed that BCMF/CMC dispersions have a critical (yield) stress and shear rate below which there cannot be steady flow under stress-controlled conditions, which is a typical

flow characteristic of thixotropic fluids. On the other hand, strain-controlled flow curves deviated from the typical picture for thixotropic fluids. To see why these differences arose, we measured flow profiles of the BCMF/CMC dispersions by rheo-MRI velocimetry. In CP geometry, where the stress variation across the gap is small (1.5%), the flow profiles were neither linear and nor showed shear banding that is expected at shear rates around the critical shear rate. Instead, there was flow throughout the gap with a highly curved velocity profile. Given the homogeneous stress distribution in the gap, the non-linearity of the profiles directly reflected differences in viscosity across the dispersions. We used a nonlocal model to describe the viscosity differences across the gap, from which we extracted a flow cooperativity length ξ of 0.08 ± 0.03 mm, comparable to floc sizes in BCMF gels without CMC. The origin of the nonlocal rheology lies in the persistence of micronscale heterogeneities that are of the order of the gap width, despite the apparent homogeneity of the dispersions at the sub-micron and macro scales. These heterogeneities have to be considered when the bulk rheology of BCMF/CMC dispersions is studied in relatively small geometries. The results of this study might also pertain to non-microfibrillated cellulosic materials in the presence of charged polymer, including foods such as ketchup and applesauce that naturally include the charged polymer pectin[43].

Acknowledgements

The authors thank Yuval Mulla, Wolf Rombouts, Jinfeng Peng, Paul Venema, Tatiana Nikolaeva (Wageningen University), Caroline Remijn, Gert-Jan Goudappel, Peter Versluis, and Donny Merkx (Unilever R&D) for their contributions. This research received funding from NanoNextNL and the Netherlands Organization for Scientific Research (NWO) in the framework of the Technology Area COAST.

References

1 D. Klemm, F. Kramer, S. Moritz, T. Lindström, M. Ankerfors, D. Gray and A. Dorris, *Angew. Chem. Int. Ed. Engl.*,

2011, **50**, 5438–5466.
2 I. Siró and D. Plackett, *Cellulose*, 2010, **17**, 459–494.
3 G. Chinga-Carrasco, *Nanoscale Research Letters*, 2011, **6**, 417.
4 N. Lavoine, I. Desloges, A. Dufresne and J. Bras, *Carbohydr. Polym.*, 2012, **90**, 735–764.
5 D. Lin, P. Lopez-Sanchez, R. Li and Z. Li, *Bioresource Technology*, 2014, **151**, 113–119.
6 S. Cousins, *Polymer*, 1995, **36**, 3885–3888.
7 A. Kuijk, R. Koppert, P. Versluis, G. van Dalen, C. Remijn, J. Hazekamp, J. Nijsse and K. P. Velikov, *Langmuir*, 2013, **29**, 14356–14360.
8 S. J. Veen, A. Kuijk, P. Versluis, H. Husken and K. P. Velikov, *Langmuir*, 2014, **30**, 13362–13368.
9 E. Saarikoski, T. Saarinen, J. Salmela and J. Seppälä, *Cellulose*, 2012, **19**, 647–659.
10 A. Karppinen, T. Saarinen, J. Salmela, A. Laukkanen, M. Nuopponen and J. Seppälä, *Cellulose*, 2012, **19**, 1807–1819.
11 T. Saarinen, S. Haavisto, A. Sorvari, J. Salmela and J. Seppälä, *Cellulose*, 2014, **21**, 1261–1275.
12 H. A. Barnes, *J. Non-Newton. Fluid*, 1995, **56**, 221–251.
13 O. Nechyporchuk, M. N. Belgacem and F. Pignon, *Carbohydr. Polym.*, 2014, **112**, 432–439.
14 F. Martoïa, C. Perge, P. J. J. Dumont, L. Orgéas, M. A. Fardin, S. Manneville and M. N. Belgacem, *Soft Matter*, 2015, **11**, 4742–4755.
15 J. D. Seymour, J. E. Maneval, K. L. McCarthy, M. J. McCarthy and R. L. Powell, *Phys. Fluids A*, 1993, **5**, 3010.
16 T. Q. Li, J. D. Seymour, R. L. Powell and M. J. McCarthy, *AIChE Journal*, 1994, **40**, 1408–1411.
17 H. Yamamoto and F. Horn, *Cellulose*, 1994, **1**, 57–66.
18 C. H. Haigler, A. R. White, R. M. Brown Jr and K. M. Cooper, *J. Cell Biol.*, 1982, **94**, 64–69.
19 H. Yan, T. Lindström and M. Christiernin, *Nord. Pulp Pap. Res. J.*, 2006, **21**, 036–043.
20 S. J. Veen, P. Versluis, A. Kuijk and K. P. Velikov, *Soft Matter*, 2015, 1–6.
21 M. Chaouche and D. L. Koch, *J. Rheol.*, 2001, **45**, 369–382.
22 M. Iotti, Ø. W. Gregersen, S. Moe and M. Lenes, *J. Polym. Environ.*, 2010, **19**, 137–145.
23 P. Coussot, Q. D. Nguyen, H. T. Huynh and D. Bonn, *J. Rheol.*, 2002, **46**, 573–17.
24 P. C. F. Møller, J. Mewis and D. Bonn, *Soft Matter*, 2006, **2**, 274–10.
25 P. C. F. Møller, S. Rodts, M. A. J. Michels and D. Bonn, *Phys. Rev. E*, 2008, **77**, 041507.
26 P. T. Callaghan, *Principles of Nuclear Magnetic Resonance Microscopy*, Oxford University Press, New York, 1993.
27 P. T. Callaghan, *Rep. Prog. Phys.*, 1999, **62**, 599–670.
28 D. W. de Kort, W. H. Rombouts, F. J. M. Hoeben, H. M. Janssen, H. Van As and J. P. M. van Duynhoven, *Macromolecules*, 2015, **48**, 7585–7591.
29 D. W. de Kort, J. P. M. van Duynhoven, F. J. M. Hoeben, H. M. Janssen and H. Van As, *Anal. Chem.*, 2014, **86**, 9229–9235.
30 D. W. de Kort, J. P. M. van Duynhoven, H. Van As and F. Mariette, *Trends Food Sci. Technol.*, 2015, **42**, 13–26.
31 N. Bourouina, D. W. de Kort, F. J. M. Hoeben, H. M. Janssen, H. Van As, J. Hohlbein, J. P. M. van Duynhoven and J. M. Kleijn, *Langmuir*, 2015, **31**, 12635–12643.
32 M. P. Lowys, J. Desbrieres and M. Rinaudo, *Food Hydrocolloids*, 2001, **15**, 25–32.
33 G. Ovarlez, S. Rodts, X. Chateau and P. Coussot, *Rheol. Acta*, 2009, **48**, 831–844.
34 J. Goyon, A. Colin, G. Ovarlez, A. Ajdari and L. Bocquet, *Nature*, 2008, **454**, 84–87.
35 G. Ovarlez, S. Cohen-Addad, K. Krishan and J. Goyon, *J. Non-Newton. Fluid*, 2013, **193**, 68–79.
36 D. C.-H. Cheng, *Br. J. Appl. Phys.*, 1966, **17**, 253–263.
37 J. Goyon, A. Colin and L. Bocquet, *Soft Matter*, 2010, **6**, 2668–11.
38 K. Kamrin and G. Koval, *Phys. Rev. Lett.*, 2012, **108**, 178301–6.
39 H. de Cagny, A. Fall, M. M. Denn and D. Bonn, *J. Rheol.*, 2015, **59**, 957–969.
40 K. Nichol, A. Zanin, R. Bastien, E. Wandersman and M. van Hecke, *Phys. Rev. Lett.*, 2010, **104**, 078302–4.
41 M. Bouzid, M. Trulsson, P. Claudin, E. Clément and B. Andreotti, *Phys. Rev. Lett.*, 2013, **111**, 238301–5.
42 J. Paredes, N. Shahidzadeh and D. Bonn, *Phys. Rev. E*, 2015, **92**, 042313.
43 B. Derakhshandeh, R. J. Kerekes, S. G. Hatzikiriakos and C. P. J. Bennington, *Chemical Engineering Science*, 2011, **66**, 3460–3470.